CHEMISTRY
A EUROPEAN JOURNAL

DOI: 10.1002/chem.200902654

# Ring-Opening Metathesis Polymerization Based Pore-Size-Selective Functionalization of Glycidyl Methacrylate Based Monolithic Media: Access to Size-Stable Nanoparticles for Ligand-Free Metal Catalysis

**Rajendar Bandari,[b] Thomas Höche,[a] Andrea Prager,[a] Klaus Dirnberger,[b] and Michael R. Buchmeiser*[a, b]**

**Abstract:** Monolithic polymeric supports have been prepared by electron-beam-triggered free-radical polymerization using a mixture of glycidyl methacrylate and trimethylolpropane triacrylate in 2-propanol, 1-dodecanol, and toluene. Under appropriate conditions, phase separation occurred, which resulted in the formation of a porous monolithic matrix that was characterized by large (convective) pores in the 30 μm range as well as pores of $<600$ nm. The epoxy groups in pores of $>7$ nm were hydrolyzed by using poly(styrenesulfonic acid) ($M_w=69400\ g\,mol^{-1}$, PDI = 2.4). The remaining epoxy groups inside pores of $<7$ nm were subjected to aminolysis with norborn-5-en-2-ylmethylamine (**2**) and provided covalently bound norborn-2-ene (NBE) groups inside these pores. These NBE groups were then treated with the first-generation Grubbs initiator [$RuCl_2(PCy_3)_2$-(CHPh)]. These immobilized Ru–alkylidenes were further used for the surface modification of the small pores by a grafting approach. A series of monomers, that is, 7-oxanorborn-5-ene-2,3-dicarboxylic anhydride (**3**), norborn-5-ene-2,3-dicarboxylic anhydride (**4**), *N*,*N*-di-2-pyridyl-7-oxanorborn-5-ene-2-carboxylic amide (**5**), *N*,*N*-di-2-pyridyl-norborn-5-ene-2-carboxamide (**6**), *N*-[2-(dimethylamino)ethyl]bicyclo-[2.2.1]hept-5-ene-2-carboxamide (**7**), and dimethyl bicyclo[2.2.1]hept-5-en-2-ylphosphonate (**8**), were used for this purpose. Finally, monoliths functionalized with poly-**5** graft polymers were used to permanently immobilize $Pd^{2+}$ and $Pt^{4+}$, respectively, inside the pores. After reduction, metal nanoparticles 2 nm in diameter were formed. The palladium-nanoparticle-loaded monoliths were used in both Heck- and Suzuki-type coupling reactions achieving turnover numbers of up to 167000 and 63000, respectively.

**Keywords:** metathesis · monoliths · nanoparticles · ring-opening polymerization · supported catalysts

## Introduction

Monolithic media, originally developed for applications in separation science,[1] have become increasingly used as catalytic supports for various (bio)catalytic reactions.[2] Monolithic polymeric supports are usually prepared within the confines of columns by a one-step, phase-separation-based process.[3] They are designed in such a way that they consist of a polymeric matrix with large, interpenetrating pores. The polymeric matrix itself is composed of interconnected, structure-forming, micro-, meso-, or macroporous microglobules. As a consequence, mass transfer between the solid phase and a secondary phase (liquid, gaseous) through the monolith is fast.[4] In the case of a catalyst attached to the surface of a meso- or macroporous monolith, high turnover frequencies, similar to those obtained under homogeneous conditions,[2d] are obtained. During the last 10 years, our group has developed numerous polymeric matrices and monolith-supported organometallic catalysts by both ring-opening metathesis polymerization (ROMP)[5] and electron-beam-triggered free-radical polymerization.[2i,6]

In this contribution we present a strategy for the synthesis of palladium and platinum nanoparticles immobilized within the confines of small pores of a monolith. The thus-prepared

[a] Dr. T. Höche, A. Prager, Prof. Dr. M. R. Buchmeiser
Leibniz Institut für Oberflächenmodifizierung e.V. (IOM)
Permoserstraße 15, 04318 Leipzig (Germany)
Fax.: (+49) 711-685-64050
E-mail: michael.buchmeiser@ipoc.uni-stuttgart.de

[b] Dr. R. Bandari, Dr. K. Dirnberger, Prof. Dr. M. R. Buchmeiser
Lehrstuhl für Makromolekulare Stoffe und Faserchemie
Institut für Polymerchemie,
Universität Stuttgart, Pfaffenwaldring 55, 7 Stuttgart (Germany)

Supporting information for this article is available on the WWW under http://dx.doi.org/10.1002/chem.200902654.

palladium nanoparticles were then used in C–C coupling reactions with high turnover numbers.

## Results and Discussion

**Synthesis and characterization of the monoliths**: Glycidyl methacrylate (GMA) based monolithic media were prepared according to published procedures.[6a] In brief, the monoliths were prepared by electron-beam (EB)-triggered free-radical polymerization using glycidyl methacrylate (GMA) as the monomer, trimethylolpropane triacrylate (TMPTA) as the cross-linker, 2-propanol and 1-dodecanol as the macroporogens, and toluene as the microporogen.[6a] Unless stated otherwise, a total dose of 22 kGy over a time period of 20 min was used (Scheme 1).

The reagents used and their amounts are summarized in Table 1 and provided monoliths with a substantial fraction (32 %) of micro- and mesopores, that is, pores with an average pore size of $<10$ nm, as evidenced by inverse size exclusion chromatography (ISEC)[7] measurements (Figure 1). The volume fraction of pores ($\varepsilon_p$), the volume fraction of interparticle void volume ($\varepsilon_z$), the total porosity ($\varepsilon_t$), the average pore diameter ($\Phi_m$), and the pore volume ($V_p$) of the parent monolith are summarized in Table 1. A scanning electron microscopy (SEM) image of the cross-section of such a monolithic structure, which did not change during modification, is shown in Figure 2.

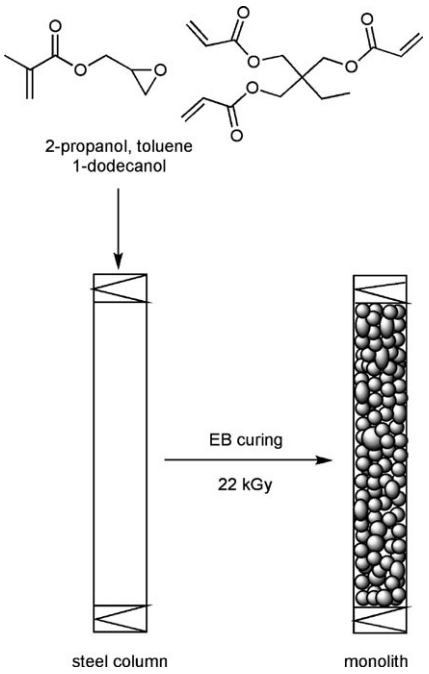


Scheme 1. Synthesis of GMA-based monoliths prepared by EB-triggered free-radical polymerization.

Table 1. Composition and structural data of the monoliths.

| Composition (in wt %) of the polymerization mixture | | | | | |
|---|---|---|---|---|---|
| GMA | TMPTA | 1-dodecanol | 2-PrOH | toluene | dose [kGy] |
| 15 | 15 | 30 | 30 | 10 | 22 |
| Structural data of the monoliths (before modification) | | | | | |
| $\varepsilon_p$ [vol %] | $\varepsilon_z$ [vol %] | $\varepsilon_t$ [vol %] | $V_p$ [μL g$^{-1}$] | $\Phi_m$ [Å] | |
| 10 | 74 | 84 | 420 | 1450 | |
| Structural data of the monoliths (after aminolysis of the epoxides) | | | | | |
| 10 | 69 | 79 | 420 | 1420 | |
| Structural data of monoliths (after ROMP-based grafting of **5**[a]) | | | | | |
| 12 | 67 | 79 | 500 | 940 | |

[a] See Table 2, entry 4.

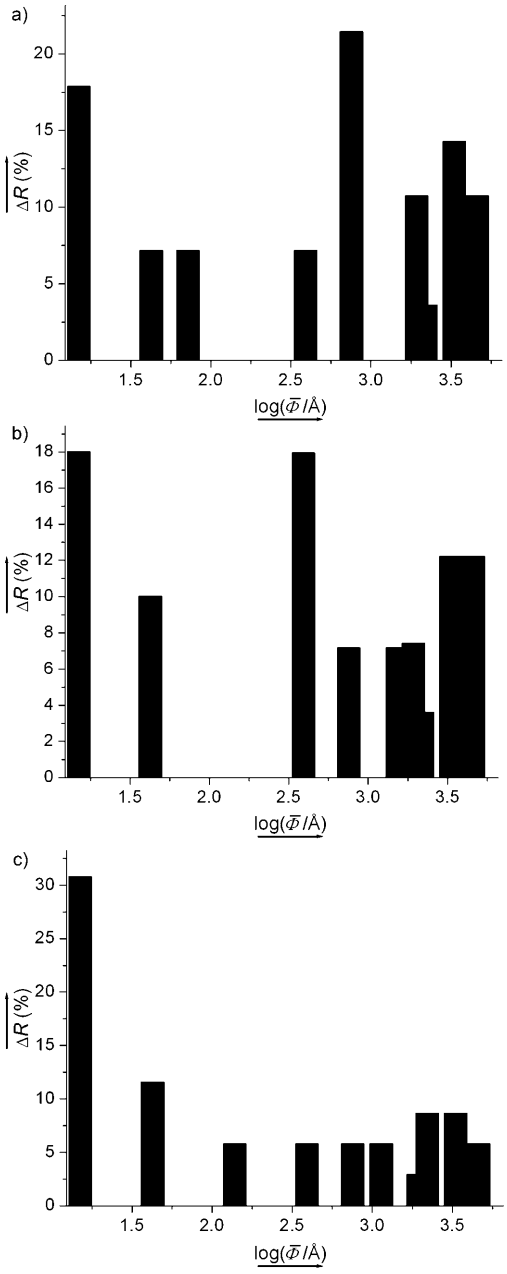


Figure 1. Graphs of $\Delta R$ versus $\log \Phi_{av}$ for a) the unmodified, b) the PSSA-modified, and c) the poly-**5** grafted monolith.

  

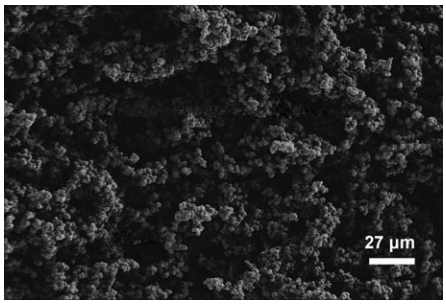


Figure 2. SEM picture of a monolith.

**Pore-size-specific modification of monoliths**: The concept of pore-size-specific modification of polymeric monoliths was first introduced by Švec and Fréchet.[8] It is based on the hydrolysis of the glycidyl methacrylate derived epoxy groups by a polymeric (acidic) reagent, for example, poly(styrenesulfonic acid). As a rule of thumb, to be penetrated by a polymer, a pore must have a diameter approximately 2.5 times larger than the hydrodynamic diameter of the polymer.[7] For the hydrolysis of the epoxy groups inside the pores, we chose a sulfonated poly(styrene) (i.e., poly(styrenesulfonic acid), PSSA) with an average $M_w$ of 69400 g mol$^{-1}$ and a PDI of 2.4 (see the Experimental Section). Based on the work of van Kreveld and Hoed[9] and of Halász and Martin,[7,10] one can calculate the exclusion diameter of a pore for such a polymer from $M_w = 10.87\Phi_r^{1.7}$ and $M_w = 2.25\Phi^{1.7}$, respectively. However, the theory is only true for narrow molecular weight distributions (PDI $\ll$ 1.1). Here, for a PSSA with a PDI of 2.4, the lowest $M_w$ that was observable in the elution peak, that is, $M_w = 3400$ g mol$^{-1}$, had to be considered and used for calculations. This value corresponds to an exclusion diameter for pores of 7 nm, that is, pores smaller than 7 nm are not penetrated by the polymer. In other words, the PSSA used should be capable of selectively hydrolyzing epoxy groups inside pores of $>7$ nm in diameter. These would be transformed into *vic*-diols whereas the epoxy groups within the small pores would remain unaffected. Because the polarity of a *vic*-diol is much higher than that of an epoxide, larger amounts of polar solvent molecules will be permanently present around these diols and the support will experience a higher degree of swelling. As a consequence, the (apparent) pore diameters will be reduced. This is exactly what was observed when the monoliths were subjected to ISEC after pore-size-selective PSSA-triggered hydrolysis of the epoxy groups. Thus, the volume fraction of pores of $\leq 7$ nm ($\log\Phi < 2$) remained virtually unchanged (within experimental error), the volume fraction of pores of around 80 nm ($\log\Phi = 2.9$) was reduced by 50%, whereas those of around 40 nm increased by 150%. The volume fraction of the larger pores ($\log\Phi > 3$) remained virtually unchanged (Figure 1). As can be seen from Table 1, the average pore diameter was slightly reduced from 145 to 142 nm.

The remaining epoxide groups located within the smaller pores ($d_p < 7$ nm) were then treated with a 10 wt% solution of norborn-5-en-2-ylmethylamine (**2**), which resulted in the covalent attachment of the norborn-2-ene groups within the small pores by aminolysis (Scheme 2).

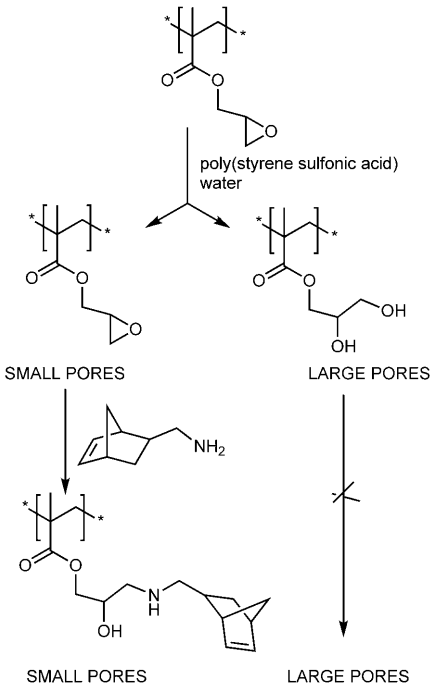


Scheme 2. Pore-size-specific modification of GMA-based monoliths.

**Functionalization by ring-opening metathesis polymerization**: Ring-opening metathesis polymerization (ROMP) is a well-established polymerization technique.[11] It entails the use of cyclic olefins with substantial ring strain, for example, norborn-2-enes and cyclooctenes.[12] The major advantages of ROMP are its truly living polymerization character[13] as well as the possibility of using functional monomers. Among the large number of well-defined initiators that are currently available, those based on ruthenium (i.e., the Grubbs initiators)[11a,14] display a higher functional group tolerance than those based on molybdenum (Schrock catalysts).[15] In the present case, ROMP-based functionalization was carried out using the first-generation Grubbs initiator [$RuCl_2(PCy_3)_2$-(CHPh)] (**1**). For this purpose, the monolith was treated with a solution of **1** in $CH_2Cl_2$ (Scheme 3). Excess initiator was removed by extensive washing of the monolithic support.

Passing solutions of different functional monomers, that is, 7-oxanorborn-5-ene-2,3-dicarboxylic anhydride (**3**), norborn-5-ene-2,3-dicarboxylic anhydride (**4**), *N*,*N*-di-2-pyridyl-7-oxanorborn-5-ene-2-carboxamide (**5**), *N*,*N*-di-2-pyridylnorborn-5-ene-2-carboxamide (**6**), *N*-[2-(dimethylamino)-ethyl]bicyclo[2.2.1]hept-5-ene-2-carboxamide (**7**), and di-

  

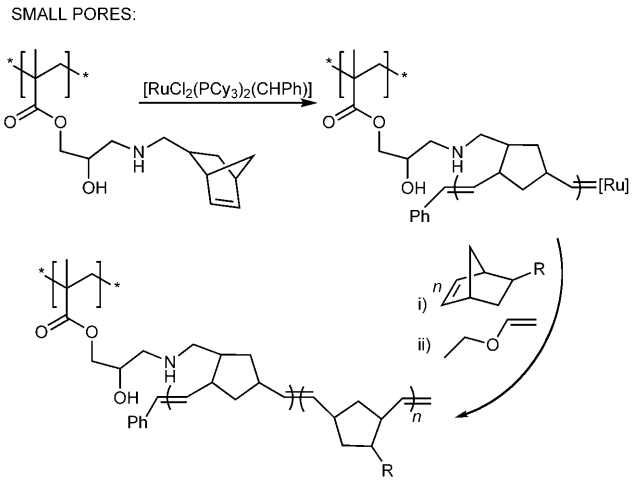


Scheme 3. Functionalization of small pores with monomers **2**–**8**.

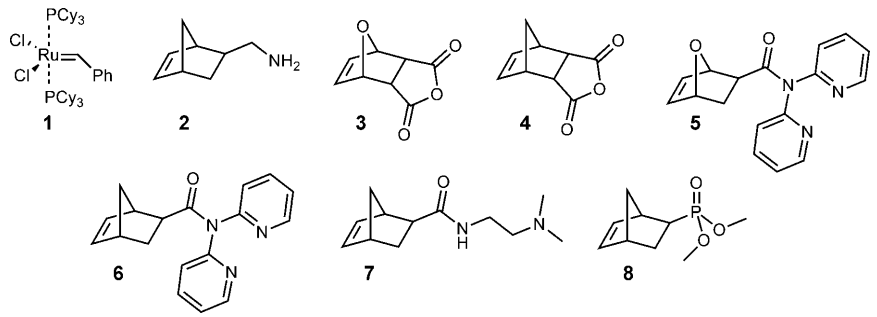


methyl bicyclo[2.2.1]hept-5-en-2-ylphosphonate (**8**), through the ruthenium-based initiator-loaded monolith resulted in the surface grafting of the monomers.

Grafting yields varied within the range of 10–420 μmol $g^{-1}$ (Table 2) and were found to depend on both the nature of the monomer and the amount of initiator immobilized on the monolith. The latter can be controlled by the amount of **2** that is immobilized on the monolithic support. The exact amount of initiator covalently bound to the monolithic support by reaction with the norborn-2-ene groups was determined by flushing the monolith with a mixture of ethyl vinyl ether (EVE, 20 vol-%) and DMSO after functionalization and collecting the effluent. These effluents were dissolved in aqua regia and the solutions were subjected to inductively coupled plasma optical emission spectrometry (ICP-OES).

Table 2. Grafting results for monomers **2**–**8**.

| Entry | Solvent | $T$ [°C] | Monomer | Grafting density [μmol $g^{-1}$] | Ru [μg $g^{-1}$] |
|---|---|---|---|---|---|
| 1 | 1,4-dioxane | 70 | **2** | 420 | 530 |
| 2 | $CH_2Cl_2$ | 40 | **3** | 220 | 60 |
| 3 | $CH_2Cl_2$ | 40 | **4** | 50 | 330 |
| 4 | $CH_2Cl_2$ | 40 | **5** | 65 | 60 |
| 5 | $CH_2Cl_2$ | 40 | **6** | 30 | 190 |
| 6 | $CH_2Cl_2$ | 40 | **7** | 145 | 500 |
| 7 | $CH_2Cl_2$ | 40 | **8** | 10 | 120 |

It is very important to note that the high permeability of the monolithic columns was preserved to a great extent during the entire modification process. Thus, the pressure drop $\Delta p$ of a 4.6×100 mm column was 4 and 8 bar ($CHCl_3$, flow rate 1 mL $min^{-1}$) prior to and after the modification process.

ISEC analysis of a monolith grafted with **5** (Table 2) revealed a significant reduction in the average pore diameter to 94 nm (Table 1). Overall, the pore size distribution (Figure 1) was shifted to smaller pore sizes. Both from the data shown in Table 1 and the graph shown in Figure 1c, it becomes evident that the surface grafting of a monolith results in graft polymers that apparently increase the fraction of small pores ($\Phi < 1.5$ nm), thus increasing the pore volume ($V_p$), at least the one that is determined by ISEC. Whether these grafted polymer chains act as "small pores" in ISEC is not fully understood and is presently the subject of further investigations.

**Immobilization of palladium and platinum within functionalized small pores**: In view of the grafting yields obtained with **5** compared with those obtained with **6**, poly-**5**-modified monoliths were used for the immobilization of both palladium and platinum. In the case of palladium, an aqueous solution of $[H_2PdCl_4]$ was prepared[16] and pumped through the functionalized monolith. For the immobilization of platinum, a 1 wt% solution of $[PtCl_4]$ in THF was passed through the monolith. Both palladium and platinum were immobilized by coordination to the di-2-pyridylamide ligand[16a] (2.7 mg Pd $g^{-1}$ and 3.8 mg Pt $g^{-1}$ of monolith as determined by ICP-OES measurements). Finally, palladium and platinum nanoparticles of $<2$ nm in diameter (Figure 3) were generated by reduction with $NaBH_4$ (Scheme 4). The chemical nature of these nanoparticles was confirmed by energy-dispersive X-ray spectrometry (EDXS) (Figure 4a and b) and both palladium and platinum were quantified by ICP-OES.

From TEM images (Figure 3a), we determined the average diameter of the palladium nanoparticles, which was found to be around 2 nm (see the Supporting Information). The density of bulk, face-centered cubic palladium is 12.03 g $cm^{-3}$.[17] Assuming the same density for our palladium nanoparticles, we calculated the density of the palladium nanoparticle as 68 atoms $nm^{-3}$. The approximate number of palladium atoms in a nanoparticle was calculated from $N_{Pd} = 68(4\pi/3)r^3$, in which $r$ is the average radius of the nanoparticles in nanometers. The weight of the palladium nanoparticle was calculated using $W_{Pd} = N_{Pd}A_{Pd}$ ($A_{Pd}$ =

  

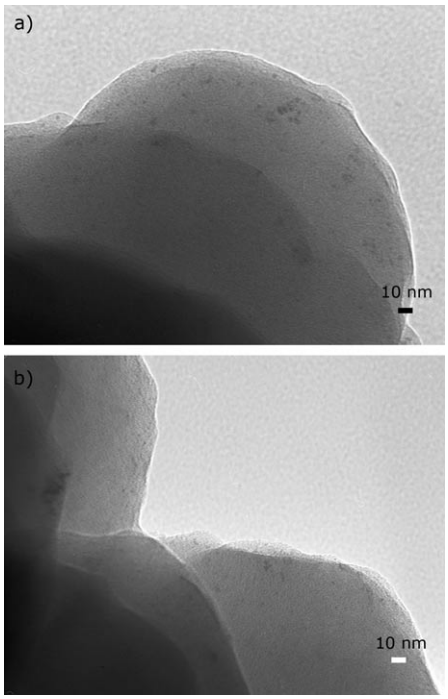


Figure 3. TEM micrographs of a) palladium and b) platinum nanoparticles formed within the small pores of a monolith.

106.4 g mol$^{-1}$, $N_{Pd}$ = number of palladium atoms). From the atomic radius of palladium (137 pm) and the average radius of the palladium nanoparticles (1 nm), we calculated the approximate number of surface palladium atoms per palladium nanoparticle. The results are summarized in Table S1 of the Supporting Information.

**Application of palladium nanoparticles in Suzuki- and Heck-type cross-coupling reactions**: Finally, the immobilized palladium nanoparticles were used as catalysts in ligand-free Suzuki-type cross-coupling reactions with various bromobenzenes and phenylboronic acid in water (Scheme 5). All the catalytic experiments were performed at a very moderate temperature of 50 °C. For all reactions, 0.64 μmol of pal-

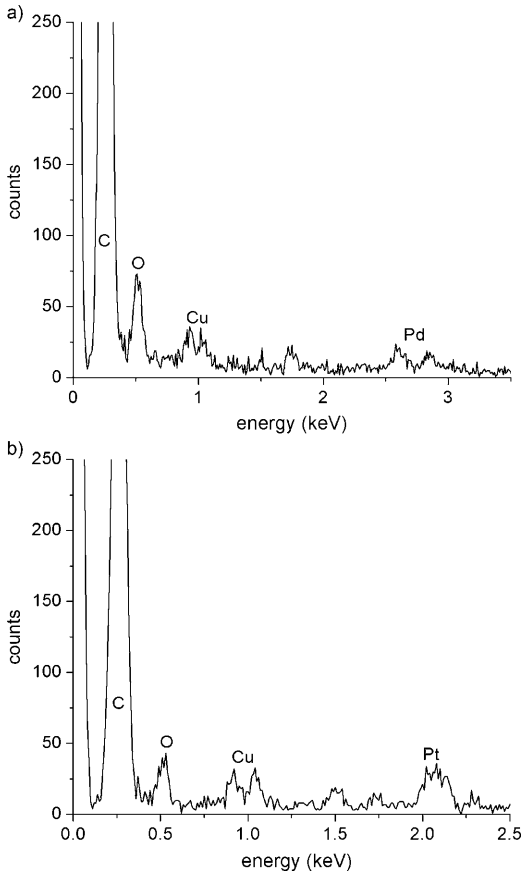


Figure 4. EDX spectra of a) palladium and b) platinum nanoparticles formed within the small pores of a poly-**5**-modified monolith. Peaks of copper result from the sample holder (copper grid).

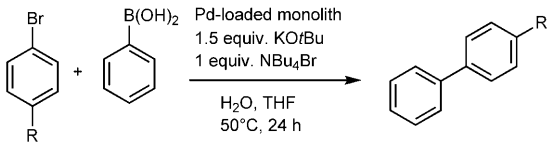


Scheme 5. Suzuki-type cross-coupling reaction using palladium nanoparticles formed within the pores of a monolith.

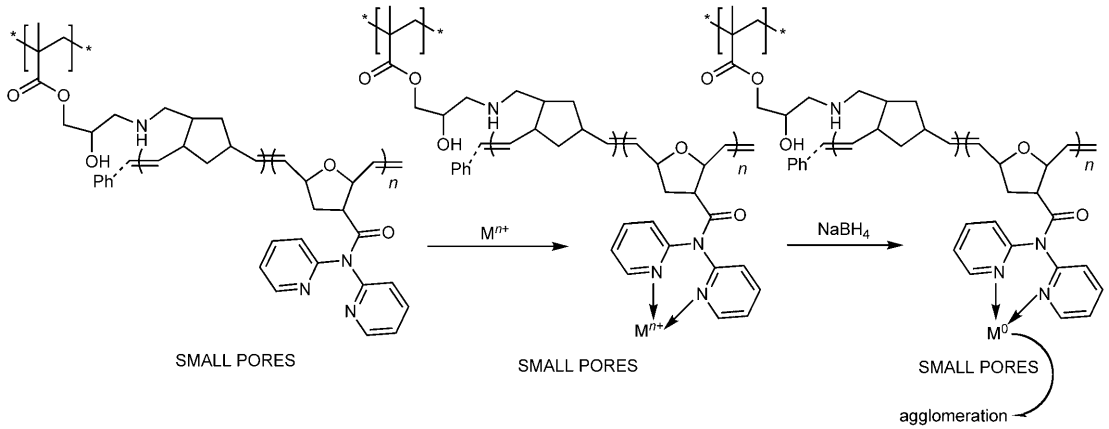


Scheme 4. Formation of palladium or platinum nanoparticles after the introduction of $Pd^{2+}$ or $Pt^{4+}$ ions and subsequent reduction with $NaBH_4$.

  

Table 3. Suzuki-type cross-coupling reactions of aryl halides and phenylboronic acid with palladium-nanoparticle-loaded monoliths.

| Substrate | Product | Conversion[a] [%] | Yield of hcp[a,b] [%] | TON[c] | TON[d] |
|---|---|---|---|---|---|
| 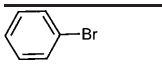 | 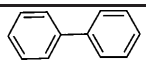 | 96 | 0 | 12300 | 61100 |
| 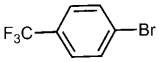 | 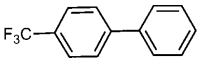 | 99 | 0 | 12800 | 63000 |
|  | 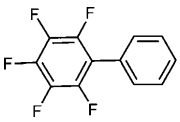 | 71 | 0.5 | 9200 | 45200 |
| 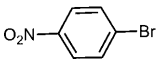 | 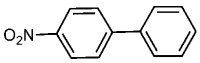 | 99 | 0 | 12800 | 63000 |
| 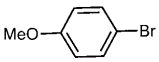 | 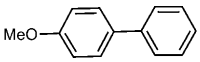 | 82 | 0.5 | 10600 | 52200 |
| 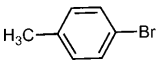 | 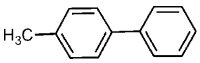 | 69 | 0.5 | 8700 | 43300 |
| 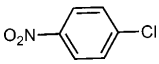 | 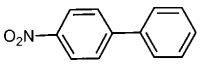 | 54 | 8 | 7000 | 34400 |

[a] Conversions and yields were determined by GC. [b] hcp = homocoupling product (biphenyl derivative). [c] Assuming every palladium atom participates in the reaction. [d] Assuming that only the surface palladium atoms participate in the reaction.

ladium and 8.2 mmol of the reactants were used. The results are summarized in Table 3.

Coupling of the aryl bromides resulted in the desired products; homocoupling was only observed to a minor extent (<0.5%). As anticipated, the highest yields were obtained with activated bromides. Turnover numbers (TONs) with respect to the number of palladium surface atoms present in all palladium nanoparticles of up to 63000 were obtained. This value is far higher than those obtained with other immobilized palladium nanoparticles.[17,18] Importantly, even activated chloroarenes could be coupled with TONs of up to 34400. After catalysis, a few palladium nanoparticles of <5 nm in diameter were generated by agglomeration and/or Ostwald-ripening of the palladium nanoparticles located at the surface of the monolith. However, the diameters of the palladium nanoparticles immobilized within the small pores remained basically constant within experimental error (Figure 5). The synthetic protocol presented here is thus a straightforward approach to the synthesis of metal nanoparticles that hardly change in size during the catalytic application despite the fact that the active species exist in different oxidation states during the catalytic cycle. This means that most palladium species that are formed in an oxidation state other than zero (i.e., $Pd^{2+}$ or $Pd^{4+}$)[19] finally re-enter the nanoparticle as $Pd^0$ species. Kinetic investigations revealed that the Suzuki-type coupling reaction was complete within 22 h. The graph of conversion versus time displays a sigmoidal shape, which is indicative of an activation process that precedes the coupling reaction (see Figure S3 of the Supporting Information). Importantly, the support can be reused at least four times without any significant change in catalytic performance (see the Supporting Information).

The immobilized palladium nanoparticles were also used as catalysts in ligand-free Heck coupling reactions using various bromobenzenes and styrene in DMF. All experiments (Scheme 6) were carried at 140°C. For all reactions, 0.33 μmol of palladium and 12.7 mmol of the reactants were used. The results are summarized in Table 4.

The coupling of the aryl bromides resulted in the desired products. Both *cis* and *trans* products were observed. As anticipated, the highest yields were obtained with activated bromides. TONs for the palladium surface atoms of the palladium nanoparticles of up to 167000 were obtained. Again, kinetic investigations were carried out and a linear graph of

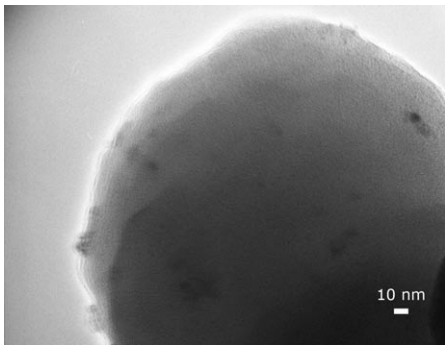


Figure 5. TEM micrograph of palladium nanoparticles after Suzuki coupling reactions.

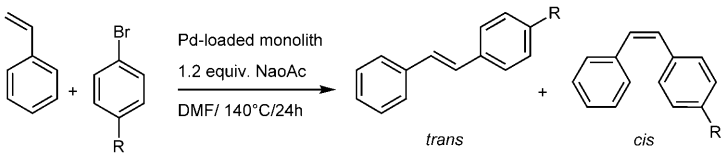


Scheme 6. Heck coupling reaction using palladium nanoparticles formed within the pores of a monolith.

  

Table 4. Heck coupling reactions of aryl bromides and styrene with palladium-nanoparticle-loaded monoliths. $\mathbf{P_1}$ = *trans*-product; $\mathbf{P_2}$ = *cis*-product.

| Halide | GC conversion [%] | | | TON[a] | TON[b] |
|---|---|---|---|---|---|
| | $\mathbf{P_1}$ (*trans*) | $\mathbf{P_2}$ (*cis*) | $\mathbf{P_1}+\mathbf{P_2}$ | | |
| 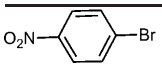 | 95 | 4 | 99 | 33900 | 167200 |
| 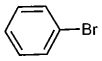 | 47 | 3 | 50 | 19300 | 95000 |
| 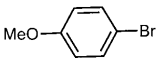 | 16 | 2 | 18 | 6900 | 34200 |

[a] Assuming every palladium atom participates in the reaction. [b] assuming that only the surface palladium atoms participate in the reaction.

conversion versus time was obtained (see Figure S4 of the Supporting Information).

**Active species**: We next turned to the question of the active species. In principle, two scenarios can be envisaged. In the first, the coupling reaction is truly heterogeneous and all reactions involve palladium species that are actually bound to the surface of nanoparticles, that is, are part thereof. The second, more likely scenario, which has also already been demonstrated for many other Heck coupling systems, is a situation in which small amounts of palladium (in the form of $Pd^0$ or ionic species[19a,20]) in the ppm range leach into the solution,[19c,21] become involved in the coupling process, and then experience different fates. Thus, in the absence of any stabilizing ligand, palladium black forms rather quickly. In case stabilizing ligands such as phosphines or di-2-pyridylamides are present, major parts of the leached palladium become stabilized again and the formation of palladium black is suppressed for a prolonged time, particularly when an excess of ligand is present.[16a]

To check for the presence of (active) palladium in solution, a palladium-loaded monolith was used in the Heck coupling reaction of bromobenzene and styrene. Then the reaction mixture was removed from the monolith, filtered, and reused for the same type of coupling reaction. Indeed, almost no reaction was observed, which indicates the absence of persistently active palladium species. ICP-OES measurements, however, revealed a palladium content of 5 ppm. Interestingly, addition of $HgCl_2$ to such a solution or to the reaction mixture in the presence of the parent monolith-supported palladium effectively suppressed any catalytic activity (see Table S1 of the Supporting Information). It is worth noting that $Hg^{II}$ is quickly reduced to $Hg^0$ in the presence of vinyl compounds such as styrene.

Similar results were obtained in Suzuki coupling reactions between phenylboronic acid and 4-trifluorobromobenzene. By using the palladium-containing solution (<4 ppm by ICP-OES) that was retrieved by filtration of a Suzuki coupling reaction catalyzed by monolith-supported palladium, no further activity was observed both in the presence and absence of $HgCl_2$ after recharging the solution with reactants, that is, phenylboronic acid and 4-trifluorobromobenzene. In contrast, when the Suzuki reaction was performed with the parent monolith-immobilized $Pd^0$ in the presence of $HgCl_2$, almost no activity was observed (2% conversion, see Table S2 of the Supporting Information).

These findings strongly suggest that 1) there are no persistently active Pd species in solution and 2) the majority of the palladium immobilized on the monolithic support is in fact $Pd^0$.[21b] Generation of the parent palladium nanoparticles within constrained geometry compartments such as pores efficiently suppresses Ostwald-ripening and thus the growth and concomitant deactivation of these nanoparticles.

## Conclusion

A novel ring-opening metathesis polymerization based approach to the pore-size-selective functionalization of electron-beam-triggered free-radical polymerization derived monoliths has been developed. This concept allows the creation and immobilization of nanoparticles within small pores. When used in catalysis, the constrained geometry of the pores effectively suppresses Ostwald-ripening, which results in a high and prolonged catalytic activity of the nanoparticles even in the absence of stabilizing ligands. Consequently, high turnover numbers in, for example, Heck- and Suzuki-type coupling reactions, are achieved.

## Experimental Section

**Materials and measurements**: $CHCl_3$, $CH_2Cl_2$, and 2-propanol were purchased from KMF Laborchemie Handels GmbH (Germany) and dried over $CaH_2$ prior to use. Methanol, 1-dodecanol, toluene, ethyl methacrylate (EMA), glycidyl methacrylate (GMA), poly(styrenesulfonic acid) (PSSA, 18 wt% in $H_2O$, $M_w$ = 69400 g mol$^{-1}$; $M_n$ = 29400 g mol$^{-1}$, PDI = 2.4), trimethylolpropane triacrylate (TMPTA), benzylidenebis(tricyclohexylphosphine)ruthenium dichloride [$(RuCl_2(PCy_3)_2(CHC_6H_5)]$ (**1**), 1,4-dioxane, bromobenzene, 1-bromo-4-nitrobenzene, 1-bromo-4-methoxybenzene, 1-bromo-4-(trifluoromethyl)benzene, 1-bromo-4-methylbenzene, 1-bromo-2,3,4,5,6-pentafluorobenzene, and 1–4-dioxane were purchased from Sigma–Aldrich (Germany). The molecular weights of PSSA (Aldrich, 561223) were determined by GPC. The GPC system consisted of a Waters 515 HPLC pump, a VDS Optilab column heater, and a Viscotek VE 3580 RI detector with the following column combination: PL aquagel-OH 30/40/50 8 μm, 300×7.5 mm (Varian Deutschland GmbH). A solution of 0.1 M $NaNO_3$, 0.01 M $NaH_2PO_4$,and 30% methanol in water was used as eluent. The flow rate was set to 0.8 mL min$^{-1}$. GPC was performed at room temperature. Calibration was carried out with poly(styrenesulfonate) sodium salt standards (Polymer Standard Service GmbH) with molecular weights of 3420—666000 g mol$^{-1}$. Monomers **2**–**8** were prepared according to published procedures.[16b,22] GC–MS investigations were carried out on a Shimadzu GCMS-QP5050 instrument equipped with an AOC-20i Autosampler and using an SPB-fused silica (Rxi-5MS) column (30 m×0.25 mm×0.25 μm film thickness) and on a Shimadzu GCMS-QP2010S instrument equipped with an AOC-20i Autosampler using an SPB-fused silica (Rxi-5MS) column (30 m×0.25 mm×0.25 μm film thickness), respectively. The injection temperature was 150 °C; the initial column temperature was set to 70 °C and then increased to 250 °C within 8.2 min. The column flow was set to 1.0 mL min$^{-1}$. NMR spectra were recorded on a Bruker Avance II+ 600 spectrometer in the solvent indicated at 25 °C and are listed in parts per million downfield from TMS as an internal standard for $^1H$ and $^{13}C$ NMR analysis. IR spectra were recorded on a Bruker Vector 22 spectrometer using ATR technology. The poly(styrene) standards ($266 < M_n < 1250000$ g mol$^{-1}$) used for inverse

  

size exclusion chromatography (ISEC) were purchased from Polymer Standards Service, PSS (Germany). The microstructures of the monolithic materials were investigated by the use of a Zeiss DSM 940A scanning electron microscope (Carl Zeiss, Oberkochen, Germany).

**Synthesis of monoliths**: All monoliths were prepared as follows: Stainless steel columns (100×4.6 mm i.d.) were cleaned, rinsed, and sonicated in a 1:1 mixture of ethanol and acetone. The columns were closed at one end with frits and end fittings. Then the columns were filled with the polymerization mixture, sealed at both ends, and irradiated. Unless stated otherwise, a total dose of 22 kGy was applied. After irradiation, the columns were directly connected to a HPLC pump and flushed with dichloromethane for 4 h at a flow rate of 0.2 mL min$^{-1}$, then with THF for 30 min at a flow rate of 0.3 mL min$^{-1}$, and finally with water for 30 min at a flow rate of 0.3 mL min$^{-1}$.

**Inverse size exclusion chromatography (ISEC)**: The volume fractions of the inter-microglobule porosity ($\varepsilon_z$), the pore porosity ($\varepsilon_p$), the total porosity ($\varepsilon_t$), the pore volume ($V_p$), and the mean pore diameter ($\Phi_m$) of the monolithic columns were characterized by ISEC[7] as described elsewhere.[6a,23]

**Hydrolysis of the epoxy groups within pores of >7 nm**: The epoxide groups of porous polymer rods were hydrolyzed by flushing the monolithic column with a solution of poly(styrenesulfonic acid) ($M_w$= 69400 g mol$^{-1}$, 4.5 wt% in water) for 15 min at a flow rate of 0.3 mL min$^{-1}$. Then the monolith was kept for 15 h at 65°C. The hydrolyzed column was then washed for 2 h at a flow rate of 0.3 mL min$^{-1}$ with water/methanol (2:1) and THF. These columns were then again characterized by ISEC.

**Functionalization of pores of <7 nm**: A typical experiment was as follows: The remaining epoxide groups within the small pores of the monolith were allowed to react with **2**. Thus, a solution containing 500 mg of **2** per 5 mL of 1,4-dioxane was introduced into the monolith, which was then kept at 60°C for 16 h. The thus modified column was then washed with 55 mL of $CH_2Cl_2$ (flow rate 0.3 mL min$^{-1}$ for 3 h). After this procedure, the monoliths were ready for ROMP-based grafting.

**Functionalization of pores of <7 nm by ROMP-based grafting**: The initiator **1** (4.0 mg, 4.86 μmol) was dissolved in $CH_2Cl_2$ (1.5 mL) and introduced into the monolith. The monolith was sealed and kept at room temperature overnight. Then the monolith was flushed with $CH_2Cl_2$ for 30 min at a flow rate of 0.3 mL min$^{-1}$ to remove any unattached catalyst and then with argon to remove all solvent. A sample of each monomer **3**–**8** (100 mg) was dissolved in $CH_2Cl_2$ (1.5 mL) and introduced into the monolith (Table 2). The monolith was sealed and kept at 40°C overnight. The following day, the monolith was flushed with a 10 vol% solution of ethyl vinyl ether (EVE) in DMSO and then with THF and kept in vacuo overnight. The amount of grafted monomer was determined by either acid–base titration (monomers **3** and **4**) or elemental analysis (nitrogen- and phosphorus-containing monomers).

**Quantification of 3 and 4**: Monoliths grafted with **3** or **4** were removed from the stainless-steel column, ground, and dried in vacuo overnight. Acid–base titrations were performed with three independent samples. Each sample was stirred for 3 days in a mixture of a standard solution of 0.1 M sodium hydroxide ($f$=1.000) and 1,4-dioxane (80:20 v/v, 10 mL). Each sample was filtered using sintered glass crucibles and washed with deionized water (15 mL). Unconsumed NaOH was back-titrated versus phenolphthalein using 0.01 M HCl ($f$=1.000).

**Preparation of palladium-loaded monoliths**: A solution of [$H_2PdCl_4$] was prepared by dissolving anhydrous $PdCl_2$ (25 mg, 0.14 mmol) in a minimum amount of HCl (37 wt%). The pH was adjusted to around 5 by the dropwise addition of an aqueous 15 wt% solution of NaOH. Finally, THF (0.2 mL) was added to enhance solvent compatibility. This solution of [$H_2PdCl_4$] (1.5 mL) was introduced into the monolith modified with poly-**5**. After introducing the [$H_2PdCl_4$] solution into the monolith, it was washed with water/THF (80:20, 20 mL). Finally, the support was dried in vacuo for 4 h and the palladium content was determined by ICP-OES.

**Preparation of platinum-loaded monoliths**: A solution of [$PtCl_4$] (15 mg, 0.077 mmol) in THF (1.5 mL) was introduced into the monolith modified with poly-**5**. Then the monolith was washed with THF (30 mL). Finally, the support was dried in vacuo for 4 h. The platinum content was determined by ICP-OES.

**Suzuki-type cross-coupling reactions**: All Suzuki-type coupling reactions were carried out in 25 mL Schlenk tubes at 50°C for 24 h. The reaction mixtures were prepared as follows: Distilled water (8 mL) and THF (8 mL) were placed in a 25 mL Schlenk tube and then the following substrates were added: *tert*-Butylbenzene (internal standard for GC–MS, 100 mg, 0.746 mmol), phenylboronic acid (1.0 g, 8.2 mmol), the aryl bromide (8.2 mmol), and KO*t*Bu (1.5 g, 12.3 mmol). Finally, tetra-*N*-butylammonium bromide (3.96 g, 12.3 mmol) was added followed by the monolithic material (0.636 μmol of palladium). After the reaction, the THF was removed under reduced pressure and the residue was dissolved in diethyl ether. The diethyl ether layer was washed with water (2× 50 mL) and saturated brine solution (2×50 mL), then dried over anhydrous $Na_2SO_4$, and concentrated under reduced pressure. The products were characterized by GC–MS and NMR and IR spectroscopy.

**Heck coupling reactions**: All Heck-coupling experiments were carried out in 25 mL Schlenk tubes at 140°C for 24 h. The reaction mixtures were prepared as follows: *N*,*N*-Dimethylformamide (DMF; 10 mL) was placed into a 25 mL Schlenk tube and then *tert*-butylbenzene (100 mg, 0.746 mmol), styrene (1.589 g, 15.28 mmol), the aryl bromide (12.7 mmol), and NaOAc (1.252 g, 15.28 mmol) were added. Finally, the monolithic material (13 mg, 0.331 μmol of palladium) was added and the mixture was degassed twice. The mixture was then stirred at the desired temperature. After completion of the reaction, the mixture was cooled to room temperature and the organic products were extracted with diethyl ether. The conversions were checked by GC—MS and NMR and IR spectroscopy.

**TEM and EDXS analyses**: The (crushed) monolithic material was dispersed in ethanol and one droplet of this suspension was applied to a carbon-coated copper grid. Then the solvent was evaporated. For bright-field TEM imaging as well as for energy-dispersive X-ray spectrometry (EDXS), a Hitachi H-8100 transmission electron microscope (operated at 200 keV at a point-to-point resolution of 0.23 nm and equipped with a $LaB_6$ filament and a STEM unit) was used. EDXS data were acquired with a Si(Li) detector with a spectral resolution of 138 eV and analyzed by using the NORAN system SIX software.

**Determination of the ruthenium, palladium, and platinum content by ICP-OES**

*Ruthenium*: The monoliths were subjected to ROMP-based functionalization as described above. EVE (20 vol-% in DMSO) was added to remove the initiator and the effluent was collected, concentrated in vacuo, and dissolved in aqua regia. The ruthenium content, which corresponds to the total amount of initiator immobilized on the monolithic surface, was quantified by ICP-OES. Ruthenium was quantified at $\lambda$= 267.876 nm by using the average of at least three consecutive measurements, the background was measured independently at $\lambda_1$=267.759 and $\lambda_2$=267.998 nm. The limit of detection (LOD) was 0.08 mg L$^{-1}$. For the calibration, aqueous ruthenium standards (pH 1, nitric acid) containing 0, 0.004, 0.14, 0.5, and 12.0 mg Ru L$^{-1}$ were used.

*Palladium and platinum*: Samples (30–40 mg) of the monoliths of interest were dissolved in a minimum amount of aqua regia (typically 5–7 mL) by applying microwave irradiation. The digest was transferred into a volumetric flask and the volume of the solution was adjusted to 10 mL. Palladium quantification was accomplished by ICP-OES at $\lambda$=340.458 nm (average of at least three consecutive measurements) and the background was measured at $\lambda_1$=340.458 and $\lambda_2$=340.955 nm. The limit of detection (LOD) was 0.014 mg L$^{-1}$. For calibration, palladium-containing aqueous standards (pH 1, nitric acid) with palladium concentrations of 0, 0.004, 0.14, 0.5, and 12.0 mg L$^{-1}$ were used. Platinum was quantified by ICP-OES at $\lambda$=214.423 nm (average of at least three consecutive measurements) and the background was measured at $\lambda_1$=214.35 and $\lambda_2$= 214.55 nm. The limit of detection (LOD) was 0.004 mg L$^{-1}$. For calibration, platinum-containing aqueous standards (pH 1, nitric acid) with platinum concentrations of 0, 0.004, 0.14, 0.5, and 12.0 mg L$^{-1}$ were used.

**Determination of palladium leaching**: To determine the palladium content in the reaction mixtures, clear filtrates were collected at the end of the reactions for precise palladium analysis. After evaporation of the sol-

  

vents, the samples were dissolved in aqua regia and the palladium was quantified as described above. An average leaching of 3% of the initial amount of palladium was observed.

## Acknowledgements

This work was supported by the Deutsche Forschungsgemeinschaft (DFG; BU 2174/1-1 and BU 2174/1-2), the Free State of Saxony and the Federal Ministry of Education and Research.

[1] a) F. Švec, T. B. Tennikova, Z. Deyl, *J. Chromatogr. Libr.* **2003**, *67*, 1; b) M. R. Buchmeiser, *Polymer* **2007**, *48*, 2187.

[2] a) S. Xie, F. Švec, J. M. J. Fréchet, *Biotechnol. Bioeng.* **1999**, *62*, 30; b) L. Yang, M. Mayr, K. Wurst, M. R. Buchmeiser, *Chem. Eur. J.* **2004**, *10*, 5761; c) J. O. Krause, K. Wurst, O. Nuyken, M. R. Buchmeiser, *Chem. Eur. J.* **2004**, *10*, 777; d) J. O. Krause, S. H. Lubbad, O. Nuyken, M. R. Buchmeiser, *Macromol. Rapid Commun.* **2003**, *24*, 875; e) M. Mayr, B. Mayr, M. R. Buchmeiser, *Angew. Chem.* **2001**, *113*, 3957; *Angew. Chem. Int. Ed.* **2001**, *40*, 3839; f) M. R. Buchmeiser, S. Lubbad, M. Mayr, K. Wurst, *Inorg. Chim. Acta* **2003**, *345*, 145; g) J. O. Krause, S. Lubbad, O. Nuyken, M. R. Buchmeiser, *Adv. Synth. Catal.* **2003**, *345*, 996; h) M. Mayr, D. Wang, R. Kröll, N. Schuler, S. Prühs, A. Fürstner, M. R. Buchmeiser, *Adv. Synth. Catal.* **2005**, *347*, 484; i) R. Bandari, W. Knolle, M. R. Buchmeiser, *Macromol. Rapid Commun.* **2007**, *28*, 2090; j) J. Krenkova, N. A. Lacher, F. Švec, *Anal. Chem.* **2009**, *81*, 2004; k) J. Krenkova, N. A. Lacher, F. Švec, *J. Chromatogr. A* **2009**, *1216*, 3252.

[3] a) M. L. Huggins, *J. Phys. Chem.* **1942**, *46*, 151; b) M. L. Huggins, *J. Am. Chem. Soc.* **1942**, *64*, 1712; c) P. J. Flory, *J. Chem. Phys.* **1942**, *10*, 51.

[4] a) A. E. Rodrigues, B. J. Ahn, A. Zoulalian, *AIChE J.* **1982**, *28*, 541; b) A. E. Rodrigues, L. Zuping, J. M. Loureiro, *Chem. Eng. Sci.* **1991**, *46*, 2765; c) A. E. Rodrigues, J. C. Lopes, Z. P. Lu, J. M. Loureiro, M. M. Dias, *J. Chromatogr.* **1992**, *590*, 93; d) A. E. Rodrigues, A. M. D. Ramos, J. M. Loureiro, M. Diaz, Z. P. Lu, *Chem. Eng. Sci.* **1992**, *47*, 4405; e) A. E. Rodrigues, Z. P. Lu, J. M. Loureiro, G. Carta, *J. Chromatogr. A* **1993**, *653*, 189; f) A. E. Rodrigues, J. M. Loureiro, C. Chenou, M. R. de La Vega, *J. Chromatogr. A* **1995**, *689–718*, 233; g) A. E. Rodrigues, *J. Chromatogr. B* **1997**, *699*, 47; h) A. E. Rodrigues, V. G. Mata, M. Zabka, L. Pais in *Monolithic Materials: Preparation and Applications*, *J. Chromatogr. Library* **2003**, *67*, edited by F. Švec, T. B. Tennikova, Z. Deyl.

[5] a) F. Sinner, M. R. Buchmeiser, *Angew. Chem.* **2000**, *112*, 1491; *Angew. Chem. Int. Ed.* **2000**, *39*, 1433; b) F. Sinner, M. R. Buchmeiser, *Macromolecules* **2000**, *33*, 5777; c) R. Bandari, A. Prager-Duschke, C. Kühnel, U. Decker, B. Schlemmer, M. R. Buchmeiser, *Macromolecules* **2006**, *39*, 5222; d) B. Schlemmer, G. Gatschelhofer, T. R. Pieber, F. M. Sinner, M. R. Buchmeiser, *J. Chromatogr. A* **2006**, *1132*, 124; e) F. M. Sinner, C. Gatschelhofer, A. Mautner, C. Magnes, M. R. Buchmeiser, T. R. Pieber, *J. Chromatogr. A* **2008**, *1191*, 274; f) A. Löber, A. Verch, B. Schlemmer, S. Höfer, B. Frerich, M. R. Buchmeiser, *Angew. Chem.* **2008**, *120*, 9278; *Angew. Chem. Int. Ed.* **2008**, *47*, 9138; g) M. R. Buchmeiser, *J. Polym. Sci., Part A* **2009**, *47*, 2219; h) C. Gatschelhofer, A. Mautner, F. Reiter, T. R. Pieber, M. R. Buchmeiser, F. M. Sinner, *J. Chromatogr. A* **2009**, *1216*, 2651.

[6] a) R. Bandari, W. Knolle, A. Prager-Duschke, M. R. Buchmeiser, *Macromol. Chem. Phys.* **2007**, *208*, 1428; b) R. Bandari, W. Knolle, M. R. Buchmeiser, *Macromol. Symp.* **2007**, *254*, 87; c) R. Bandari, C. Elsner, W. Knolle, C. Kühnel, U. Decker, M. R. Buchmeiser, *J. Sep. Sci.* **2007**, *30*, 2821; d) R. Bandari, W. Knolle, M. R. Buchmeiser, *J. Chromatogr. A* **2008**, *1191*, 268.

[7] I. Halász, K. Martin, *Angew. Chem.* **1978**, *90*, 954; *Angew. Chem. Int. Ed. Engl.* **1978**, *17*, 901.

[8] a) F. Švec, J. M. J. Fréchet, *Adv. Mater.* **1994**, *6*, 242; b) F. Švec, J. M. J. Fréchet, *Int. Lab.* **1997**, *27*, 12A; c) F. Švec, J. M. J. Fréchet, *Science* **1996**, *273*, 205.

[9] M. E. Van Kreveld, V. D. Hoed, *J. Chromatogr.* **1973**, *83*, 111.

[10] I. Halász, K. Martin, *Ber. Bunsen-Ges.* **1975**, *79*, 731.

[11] a) R. H. Grubbs, *Handbook of Methathesis, Vol. 1–3*, 1st ed. (Ed.: R. H. Grubbs), Wiley-VCH, Weinheim, **2003**; b) C. W. Bielawski, R. H. Grubbs, *Adv. Polym. Sci.* **2007**, *32*, 1.

[12] M. R. Buchmeiser in *Handbook of Ring-Opening Polymerization*, 1st ed. (Eds.: P. Dubois, O. Coulembier, J.-M. Raquez), Wiley-VCH, Weinheim, **2009**, p. 197.

[13] K. Matyjaszewski, *Macromolecules* **1993**, *26*, 1787.

[14] T. M. Trnka, R. H. Grubbs, *Acc. Chem. Res.* **2001**, *34*, 18.

[15] M. R. Buchmeiser, *Chem. Rev.* **2000**, *100*, 1565.

[16] a) M. R. Buchmeiser, K. Wurst, *J. Am. Chem. Soc.* **1999**, *121*, 11101; b) M. R. Buchmeiser, S. Lubbad, M. Mayr, K. Wurst, *Inorg. Chim. Acta* **2003**, *345*, 145.

[17] a) K. R. Gopidas, J. K. Whitesell, M. A. Fox, *Nano Lett.* **2003**, *3*, 1757; b) K. R. Gopidas, J. K. Whitesell, M. A. Fox, *J. Am. Chem. Soc.* **2003**, *125*, 6491.

[18] C. Ornelas, A. K. Diallo, J. Ruiz, D. Astruc, *Adv. Synth. Catal.* **2009**, *351*, 2147.

[19] a) C. Amatore, A. Jutand, *Acc. Chem. Res.* **2000**, *33*, 314; b) M. T. Reetz, J. G. de Vries, *Chem. Commun.* **2004**, 1559; c) J. G. de Vries, *Dalton Trans.* **2006**, 421.

[20] a) C. Amatore, M. Azzabi, A. Jutand, *J. Am. Chem. Soc.* **1991**, *113*, 8375; b) C. Amatore, E. Carré, A. Jutand, M. A. M′Barki, *Organometallics* **1995**, *14*, 1818; c) C. Amatore, A. Jutand, M. A. M′Barki, *Organometallics* **1992**, *11*, 3009; d) A. Jutand, *Eur. J. Inorg. Chem.* **2003**, 2017; e) A. Jutand, S. Négri, *Organometallics* **2003**, *22*, 4229.

[21] a) A. V. Gaikwad, A. Holuigue, M. B. Thathagar, J. E. ten Elshof, G. Rothenberg, *Chem. Eur. J.* **2007**, *13*, 6908; b) N. T. S. Phan, M. Van der Sluys, C. W. Jones, *Adv. Synth. Catal.* **2006**, *348*, 609; c) L. Durán Pachón, G. Rothenberg, *Appl. Organomet. Chem.* **2008**, *22*, 288.

[22] a) R. Bandari, W. Knolle, A. Prager-Duschke, M. R. Buchmeiser, *Macromol. Rapid Commun.* **2007**, *28*, 2090; b) F. Sinner, M. R. Buchmeiser, R. Tessadri, M. Mupa, K. Wurst, G. K. Bonn, *J. Am. Chem. Soc.* **1998**, *120*, 2790; c) Y. S. Vygodskii, A. S. Shaplov, E. I. Lozinskaya, O. A. Filippov, E. S. Shubina, R. Bandari, M. R. Buchmeiser, *Macromolecules* **2006**, *39*, 7821.

[23] B. Scheibitz, A. Prager, M. R. Buchmeiser, *Macromolecules* **2009**, *42*, 3493.

Received: September 27, 2009
Revised: January 13, 2010
Published online: March 12, 2010

  